# Frequency Tunable Impedance Matching Nonreciprocal Bandpass Filter Using Time-Modulated Quarter-Wave Resonators

Girdhari Chaudhary, *Member, IEEE*, and Yongchae Jeong, *Senior Member, IEEE*

***Abstract*—In this article, we present a frequency tunable magnetless nonreciprocal bandpass filter (BPF) that uses time-modulated quarter-wave microstrip line resonators. The proposed nonreciprocal BPF can transform real-to-real, real-to-complex, and complex-to-complex termination impedances. To achieve nonreciprocity, a modulation signal is directly applied to the varactor through the transmission line. The modulation scheme in the proposed nonreciprocal BPF, while simple, nevertheless achieves an excellent nonreciprocal response. The center frequency ($f_0$) and nonreciprocal response of the proposed BPF are tuned by changing the dc bias voltage of the varactor. The design is validated by experiments using four prototypes of nonreciprocal BPFs (filter A: 50-to-50 Ω, filter B: 20-to-50 Ω, filter C: 25+$j$10-to-50 Ω, and filter D: 25+$j$10-to-55+$j$10 Ω). The measured results confirm that the $f_0$ of the nonreciprocal BPF is tuned from 1.64 to 1.97 GHz (330 MHz) with a forward insertion loss variation of 4.96 to 3.94 dB and backward isolation of 20 dB over a bandwidth of 50 MHz.**

***Index Terms*—Bandpass filter (BPF), frequency tunable, impedance matching, isolator, magnetless nonreciprocal filter.**

## I. Introduction

Nonreciprocal components, such as circulators and isolators, are crucial to modern wireless communication systems as they are widely employed to protect active devices from unwanted reflected signals or achieve self-interference cancelation in the in-band full duplex systems [1]–[3]. Nonreciprocal circuits are traditionally almost entirely based on the magnetic biasing of ferrite materials. They are cumbersome, costly, and unsuitable for use with integrated circuits [4], [5]. To eliminate need for a magnet, active and nonlinear circuits have been attempted with the goal of achieving nonreciprocity; however, these approaches suffer from poor noise figure, limited power handling, and small dynamic range [6]–[8].

Recent years have seen a groundswell of interest in the creation of magnetless nonreciprocal circuits due to the increasing need for miniaturized, integratable, and affordable technologies. Linear periodically time-varying circuits have been prescribed as a means of achieving magnetless circulators and isolators. The circuit size of magnetless circulators has reduced through the use of three spatiotemporally modulated three lumped-element *LC* resonators, in either a Δ- or Y-topology, [9]–[12]. Magnetless gyrators with a 180° nonreciprocal phase shift have been realized using a staggered commutation network by sequentially switching between the transmission and receiving paths, which was embedded inside a $3/4\lambda_g$ ring resonator to create a magnetless circulator in complementary metal–oxide–semiconductor technology [13].

Magnetless nonreciprocal bandpass filters (BPFs) that allow a signal to travel in only one direction using spatiotemporal modulation (STM) with time-modulated resonators were reported in [14]. Wu *et al.* [14]–[16] presented lumped-element coupled-resonator nonreciprocal BPFs using time-modulated capacitors. A time-varying coupling matrix approach was generalized in [17] to design the nonreciprocal BPF. With design, the modulation and RF signals were separated using a low-pass filter and a static dc block capacitor and implemented of an additional bias circuit and added duplexing circuits resulted in an increase in the overall insertion loss (IL). Wu *et al.* [18] reported a two-pole microstrip line nonreciprocal BPF based on $\lambda_g/2$ resonators. In this design, the modulation signal was directly loaded into $\lambda_g/2$ resonators. Wu *et al.* [19] extended this design to directly connect an ac voltage modulation signal through a single inductor.

Despite substantial research, the conventional nonreciprocal BPFs continue to be based on 50-to-50 Ω RF port termination impedances, no previous work has successfully implemented a multifunctional (e.g., capable of simultaneous impedance matching and frequency tuning) nonreciprocal BPF in a single device.

In this article, we present frequency tunable magnetless nonreciprocal BPF with arbitrarily termination impedances using time-modulated quarter-wave ($\lambda_g/4$) resonators. To achieve

Manuscript received May 20, 2021; revised June 30, 2021 and July 21, 2021; accepted August 7, 2021. Date of publication August 25, 2021; date of current version March 1, 2022. This work was supported in part by the National Research Foundation (NRF) of Korea, funded by the Korea Government (MSIT) under Grant 2020R1A2C2012057 and in part by the Basic Science Research Program through the NRF of Korea, funded by the Ministry of Education under Grant 2019R1A6A1A09031717. *(Corresponding author: Yongchae Jeong.)*

The authors are with the Division of Electronics Engineering, IT Convergence Research Center, Jeonbuk National University, Jeonju-si 54896, South Korea (e-mail: girdharic@jbnu.ac.kr; ycjeong@jbnu.ac.kr).

Color versions of one or more figures in this article are available at https://doi.org/10.1109/TIE.2021.3106023.
Digital Object Identifier 10.1109/TIE.2021.3106023

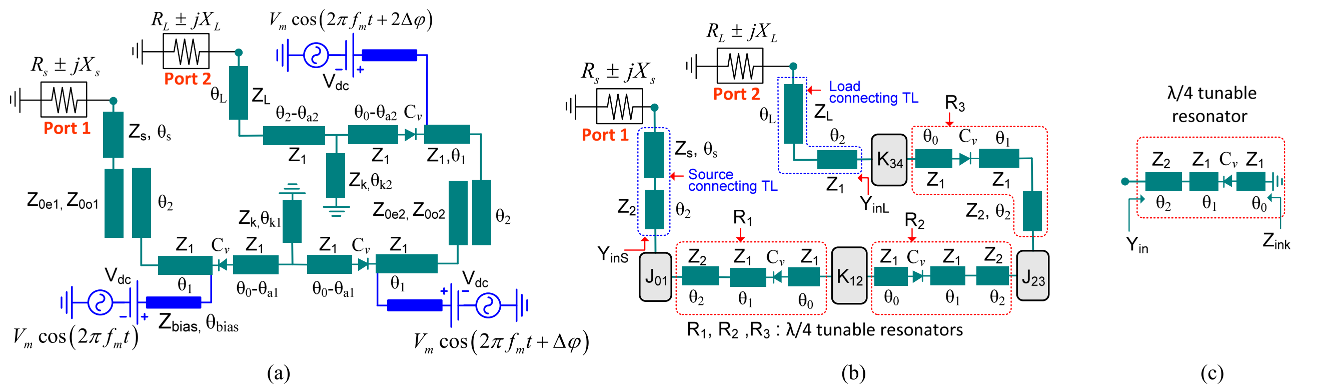


Fig. 1. (a) Proposed structure of a three-pole nonreciprocal BPF. (b) Equivalent BPF circuit without modulation. (c) Structure of tunable resonator.

nonreciprocity, the modulation signal was directly connected to the varactor through a bias transmission line (TL), which simplified the practical implementation of the modulation bias circuit.

## II. Design Theory

Fig. 1(a) shows a structure of the proposed frequency tunable nonreciprocal BPF. The source and load impedances of the nonreciprocal BPF are terminated with complex impedance $Z_{\text{source}} = R_S \pm jX_S$ and $Z_{\text{load}} = R_L \pm jX_L$, respectively, where $R_S$ and $R_L$ are the real parts and $X_S$ and $X_L$ are the imaginary parts of the source and load impedances. The proposed nonreciprocal BPF can be designed with either real-to-real, real-to-complex, or complex-to-complex termination impedances according to the design requirements. To achieve a magnetless nonreciprocal BPF ($|S_{21}| \neq |S_{12}|$) based on STM, the resonators are modulated in time and space by modulating the capacitors as follows:

$$C_v(t) = C_0 + \Delta C \cos(2\pi f_m t + \Delta\varphi) \tag{1}$$

where $C_0$ is the nominal capacitance, $\Delta C$ is the modulation depth, $f_m$ is the modulation frequency, and $\Delta\varphi$ is the progressive phase shift of the modulation signal [14].

In the proposed design, the modulation signal was directly connected to the varactor diode through TL with the characteristic impedance of $Z_{\text{bias}}$ and electrical length of $\theta_{\text{bias}}$. Intermodulation (IM) products are generated when the capacitors $C_v$ are modulated sinusoidally with progressive phase shift $\Delta\varphi$. Using proper modulation parameters ($\Delta C, f_m$, and $\Delta\varphi$), the powers at IM products can be collected back at the RF carrier frequency constructively to provide a small forward transmission loss or added up destructively in the reverse direction to create high isolation.

### A. Analytical Analysis of BPF Without Modulation

Fig. 1(b) shows the corresponding BPF without modulation. The parallel-coupled lines are equivalent to $J$ inverters, whereas the T-type TLs are equivalent to $K$ inverters. The TL with $Z_S = 1/Y_S$ and $\theta_S$ is connected at the source, while the TL with $Z_L = 1/Y_L$ and $\theta_L$ is connected at the load. These TLs are used to transform the complex impedance of the source/load to real impedance at the first and last inverters. Using filter theory [20], the values of the $J/K$-inverter are determined as follows:

$$J_{01} = \sqrt{\frac{\text{Re}(Y_{inS})\,\Delta b}{g_0 g_1}}, \quad K_{34} = \sqrt{\frac{x\Delta}{\text{Re}(Y_{inL}) g_3 g_4}} \tag{2a}$$

$$K_{12} = \frac{\Delta x}{\sqrt{g_1 g_2}}, \quad J_{23} = \frac{b\Delta}{\sqrt{g_2 g_3}} \tag{2b}$$

where $g_i$ is the value of low-pass prototype element and $\Delta$ is the equiripple fractional bandwidth.

Similarly, $\text{Re}(Y_{inS})$ and $\text{Re}(Y_{inL})$ are the real part of input admittance at the first and last inverters, respectively, as shown in Fig. 1(b).

### B. Resonant Frequency and Slope Parameter of Resonator

Fig. 1(c) shows the proposed structure of the tunable $\lambda_g/4$ resonator. The resonator consists of three TLs with characteristic impedances and electrical lengths of $Z_1, Z_2, \theta_0, \theta_1$, and $\theta_2$ and a varactor diode with a static capacitance of $C_v$ at a specific dc bias voltage. The input admittance looking toward the short-circuit TL is calculated as follows:

$$Y_{in} = jY_2 \frac{A_1 + Y_2 \tan\{\theta_2\omega/\omega_{\text{ref}}\}}{Y_2 - A_1 \tan\{\theta_2\omega/\omega_{\text{ref}}\}} \tag{3}$$

where

$$A_1 = Y_1 \frac{A_2 + Y_1 \tan\{\theta_1\omega/\omega_{\text{ref}}\}}{Y_1 - A_2 \tan\{\theta_1\omega/\omega_{\text{ref}}\}} \tag{4a}$$

$$A_2 = \frac{\omega C_v Y_1 \cot\{\theta_0\omega/\omega_{\text{ref}}\}}{Y_1 \cot\{\theta_0\omega/\omega_{\text{ref}}\} - \omega C_v}, \quad Y_1 = \frac{1}{Z_1}, \quad Y_2 = \frac{1}{Z_2} \tag{4b}$$

and $\omega$ is the operating frequency of the resonator, while $\omega_{\text{ref}}$ is the frequency at which the electrical lengths ($\theta_0$, $\theta_1$, and $\theta_2$) of the TLs are defined. Similarly, the input impedance of the resonator looking toward the open-circuited TL is determined as follows:

$$Z_{ink} = jZ_1 \frac{A_3 + Z_1 \tan\{\theta_0\omega/\omega_{\text{ref}}\}}{Z_1 - A_3 \tan\{\theta_0\omega/\omega_{\text{ref}}\}} \tag{5}$$

where

$$A_3 = Z_1 \frac{Z_1 \tan\{\theta_1\omega/\omega_{\text{ref}}\} - Z_2 \cot\{\theta_2\omega/\omega_{\text{ref}}\}}{Z_1 + Z_2 \cot\{\theta_2\omega/\omega_{\text{ref}}\} \tan\{\theta_1\omega/\omega_{\text{ref}}\}} - \frac{1}{\omega C_v}. \tag{6}$$

The resonant angular frequency $\omega_0$ can be established by setting $B = \text{im}(Y_{in}) = 0$ or $X = \text{im}(Z_{ink}) = 0$. Likewise, the susceptance slope parameter ($b$) and reactance slope parameter ($x$) of the resonator at resonant frequency $\omega_0$ can be found as follows:

$$b = \frac{\omega_0}{2}\frac{dB}{d\omega}\bigg|_{\omega=\omega_0}, \quad x = \frac{\omega_0}{2}\frac{dX}{d\omega}\bigg|_{\omega=\omega_0} \tag{7}$$

where $B = \text{im}(Y_{in})$ is the susceptance and $X = \text{im}(Z_{ink})$ is the reactance of the proposed resonator.

## C. Analysis of Source and Load Connecting TL

The electrical length $\theta_{S,L}$ of the source/load connecting the TL that can transform $Z_{\text{source}} = R_s \pm jX_S$ or $Z_{\text{load}} = R_L \pm jX_L$ to purely real impedance at $\omega_0$ looking at the first or last *J*-inverter can be derived through the following equation, where subscript $s$ is the source, and $L$ is the load port:

$$\theta_{s,L}|_{\omega_{\text{ref}}} = \frac{\omega_{\text{ref}}}{\omega_0}\tan^{-1}\left(\frac{-k_2 \pm \sqrt{k_2^2 - 4k_1k_3}}{2k_1}\right) \tag{8}$$

where

$$k_1 = Y_{s,L}^2 X_{s,L} B_1 - Y_{s,L}^4\left(R_{s,L}^2 + X_{s,L}^2\right)\tan\{\theta_2\omega_0/\omega_{\text{ref}}\} + B_2 \tag{9a}$$

$$k_2 = Y_{s,L}\left[B_1B_3 + 2X_{s,L}B_2 + 2X_{s,L}Y_{s,L}^2\tan\{\theta_2\omega_0/\omega_{\text{ref}}\}\right] \tag{9b}$$

$$k_3 = Y_{s,L}^2\left[B_2\left(R_{s,L}^2 + X_{s,L}^2\right) - X_{s,L}B_1 - \tan\{\theta_2\omega_0/\omega_{\text{ref}}\}\right] \tag{9c}$$

$$B_1 = Y_2\left(1 - \tan^2\{\theta_2\omega_0/\omega_{\text{ref}}\}\right) \tag{9d}$$

$$B_2 = Y_2^2\tan^2\{\theta_2\omega_0/\omega_{\text{ref}}\}, \quad B_3 = R_{s,L}^2 + X_{s,L}^2 - 1. \tag{9e}$$

Once $\theta_{S,L}$ is calculated, the value of $\text{Re}(Y_{inS,\,L})$ can be determined using the information from the first and last inverters as well as the following equations:

$$\text{Re}(Y_{inS,L}) = Y_2\frac{\alpha_1\alpha_2 + \alpha_3\alpha_4}{\alpha_1^2 + \alpha_4^2} \tag{10}$$

where

$$\alpha_1 = R_{s,L}Y_2Y_{s,L} - Y_{s,L}^2R_{s,L}\tan\{\theta_2\omega_0/\omega_{\text{ref}}\}\tan\{\theta_{s,L}\omega_0/\omega_{\text{ref}}\} \tag{11a}$$

$$\alpha_2 = \left\{\begin{matrix} Y_{s,L} - Y_{s,L}X_{s,L}\tan\{\theta_{s,L}\omega_0/\omega_{\text{ref}}\}(Y_{s,L} - Y_2) \\ -Y_2\tan\{\theta_2\omega_0/\omega_{\text{ref}}\}\tan\{\theta_{s,L}\omega_0/\omega_{\text{ref}}\}\end{matrix}\right\} \tag{11b}$$

$$\alpha_3 = Y_{s,L}^2R_{s,L}\tan\{\theta_{s,L}\omega_0/\omega_{\text{ref}}\} + Y_2R_{s,L}Y_{s,L}\tan\{\theta_2\omega_0/\omega_{\text{ref}}\} \tag{11c}$$

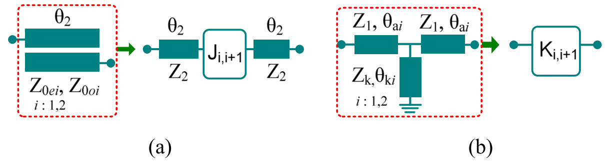


Fig. 2. Implementation of *J*/*K* inverters. (a) Parallel-coupled line as *J*-inverter. (b) T-type TL as a *K*-inverter.

$$\alpha_4 = \left\{\frac{\begin{matrix} Y_2\left[X_{s,L}Y_{s,L} + \tan\{\theta_2\omega_0/\omega_{\text{ref}}\}\right] \\ + \tan\{\theta_{2,L_1}\omega_0/\omega_{\text{ref}}\}\end{matrix}}{\left[Y_{s,L} - Y_{s,L}^2X_{s,L}\tan\{\theta_2\omega_0/\omega_{\text{ref}}\}\right]}\right\}. \tag{11d}$$

## D. Implementation of J/K Inverters

Fig. 2(a) shows a *J*-inverter with two connected TLs ($Z_2$ and $\theta_2$), which can be practically implemented using parallel-coupled lines with open-circuit stubs [20], [21]. The even- and odd-mode impedances ($Z_{0ei}$ and $Z_{0oi}$) of the parallel-coupled line with arbitrary electrical length $\theta_2$ and characteristic impedance $Z_2$ are provided through the following:

$$Z_{0ei} = Z_2\frac{1 + J_{i,i+1}Z_2\csc(\theta_2\omega_0/\omega_{\text{ref}}) + J_{i,i+1}^2Z_2^2}{1 - J_{i,i+1}^2Z_2^2\cot^2(\theta_2\omega_0/\omega_{\text{ref}})} \tag{12a}$$

$$Z_{0oi} = Z_2\frac{1 - J_{i,i+1}Z_2\csc(\theta_2\omega_0/\omega_{\text{ref}}) + J_{i,i+1}^2Z_2^2}{1 - J_{i,i+1}^2Z_2^2\cot^2(\theta_2\omega_0/\omega_{\text{ref}})}. \tag{12b}$$

Fig. 2(b) shows a *K*-inverter implementation with T-type TLs. The T-type *K*-inverter consists of a series TL with characteristic impedance $Z_1$ and electrical length $\theta_{ai}$ as well as a shunt short-circuited TL with characteristic impedance $Z_k$ and electrical length $\theta_{ki}$. The circuit parameters of the T-type *K*-inverter can be derived by equating the *ABCD* parameters of the *K*-inverter and its T-type equivalent circuit through the following equations:

$$\theta_{ai}|_{\omega=\omega_{\text{ref}}} = -\frac{\omega_{\text{ref}}}{\omega_0}\tan^{-1}\left(\frac{K_{i,i+1}}{Z_1}\right) \tag{13a}$$

$$\theta_{ki}|_{\omega=\omega_{\text{ref}}} = \frac{\omega_{\text{ref}}}{\omega_0}\tan^{-1}\left\{\frac{K_{i,i+1}Z_1^2}{Z_1^2Z_k - K_{i,i+1}^2Z_k}\right\}. \tag{13b}$$

Because the characteristic impedance $Z_1$ of series TLs is identical to the characteristic impedance of the resonator, negative electrical length $\theta_{ai}$ will be compensated within resonator electrical length $\theta_0$. Consequently, the resonator's electrical length will be shorter than the original length, as shown in Fig. 1(b).

## E. Design Method

The proposed nonreciprocal BPF was designed pursuant to the following steps.

1) The BPF design process begins by setting BPF specifications, such as the passband ripple (RL), equiripple bandwidth FBW ($\Delta$), $Z_{\text{source}} = R_S \pm jX_S$, $Z_{\text{load}} = R_L \pm jX_L$, $Z_2$, $Z_1$, $\theta_2$, $\theta_1$, $\theta_0$, $Z_k$, $Z_S$, $Z_L$, $C_v$, and $f_{\text{ref}}$.

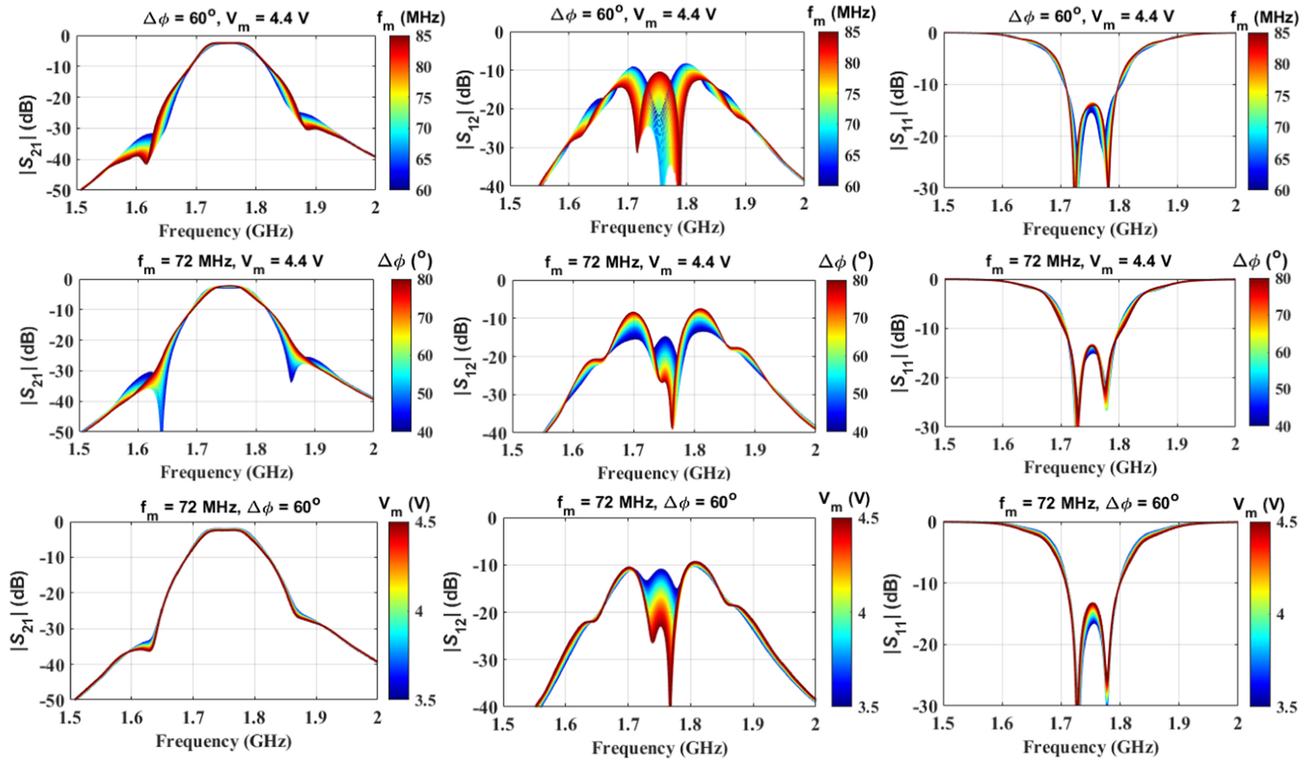


Fig. 3. Parametric studies of third-order magnetless nonreciprocal BPF with $R_S = 20\ \Omega$, $X_S = 0$, $R_L = 50\ \Omega$, $X_L = 0$, and $V_{\mathrm{dc}} = 17.5$ V with a 1T362 varactor diode manufactured by Sony, Inc., and different modulation parameters. Varactor diode is biased at $V_{\mathrm{dc}} = 17.5$ V to set nominal capacitance.

2) Calculate the resonant frequency ($f_0$) by setting $B = \mathrm{im}\,(Y_{in}) = 0$ in (3) or $X = \mathrm{im}\,(Z_{ink}) = 0$ in (5). Similarly, the susceptance slope parameter $b$ and reactance slope parameter $x$ are calculated using (7).
3) Calculate $\theta_S$ and $\theta_L$ at $f_{\mathrm{ref}}$ using (8) and (9), respectively. Once $\theta_S$ and $\theta_L$ are obtained, then calculate the values of $\mathrm{Re}(Y_{inS})$ and $R(Y_{inL})$ using (10) and (11).
4) Calculate the *J*- and *K*-inverter values using (2).
5) After obtaining *J*-inverter values, calculate the even- and odd-mode impedances of the parallel-coupled line using (12).
6) For practical implementation of the *K*-inverter, calculate $\theta_{ai}$ and $\theta_{ki}$ using (13). The negative electrical length $\theta_{ai}$ is compensated within $\theta_0$, with the result that $\theta_0$ is lower than the original value.
7) To achieve the desired nonreciprocal BPF response, the modulation parameter ($f_m$, $\Delta\varphi$, and $V_m$) should be obtained by parametric studies. Modulation frequency $f_m$ should be set close to the equiripple bandwidth ($\Delta$), while $\Delta\varphi$ should be in the range of 45° to 70°.

To validate the theoretical analysis of the proposed nonreciprocal BPF, we performed parametric studies at modulation frequencies $f_m$, progressive phase shifts $\Delta\varphi$, and amplitude of modulation signals $V_m$. Fig. 3 shows the results of parametric studies. In this demonstration, the BPF was designed for 0.043 dB Chebyshev filter response with a center frequency of 1.80 GHz and a static equiripple bandwidth of 75 MHz. The circuit parameters are given in Table I. The parametric studies were performed using a varactor 1T362 SPICE model manufactured by Sony Corporation [22]. The time-varying capacitors were implemented with reverse biased varactor diodes.

TABLE I
Calculated Circuit Parameters

| $R_S = 20\ \Omega$, $X_S = 0$, $R_L = 50\ \Omega$, $\Delta = 5\%$, passband ripple = 0.043 dB | | | |
|---|---|---|---|
| $Z_1 = 70\ \Omega$, $Z_2 = 60\ \Omega$ $C_v = 8$ pF, $\theta_2 = 25°$, $\theta_1 = 40°$, $\theta_0 = 16°$, $f_{ref} = 1.5$ GHz | | | |
| $Z_S/Z_L/Z_k/Z_{\mathrm{bias}}$ (Ω) | $\theta_S/\theta_L$ (°) | $\theta_{a1}/\theta_{a2}$ (°) | $\theta_{k1}/\theta_{k2}/\theta_{bias}$ (°) |
| 70/70/70/100 | 48.22/52.14 | -2.20/-12.63 | 2.20/13.2/75 |
| $Z_{0e1}/Z_{0o1}$ (Ω) | | $Z_{0e2}/Z_{0o2}$ (Ω) | |
| 78.6044/48.5798 | | 66.2885/54.8032 | |

Bias voltage $V_{\mathrm{dc}}$ was provided for each varactor to set the nominal capacitance. The modulation signal was applied directly to the varactor through TL with a characteristic impedance of 100 Ω and electrical length of 75°. The results were obtained by using the Keysight Advanced Design System (ADS) ideal built-in models in conjunction with large-signal scattering parameters analysis modules. As shown in Fig. 3, the proposed modulated BPF exhibited nonreciprocal BPF response during the various combinations of $f_m$, $\Delta\varphi$, and $V_m$.

When $f_m$ is approximately equal to equiripple bandwidth (e.g., 74 MHz), the BPF exhibited reverse isolation ($|S_{12}|$) with minimum forward IL ($|S_{21}|$). Similarly, when $f_m$ was slightly higher than the equiripple bandwidth (e.g., 85 MHz), the bandwidth of the reverse isolation increased, although isolation magnitude at $f_0$ decreased. When $f_m$ was slightly lower than 72 MHz, the number of poles in reverse isolation was reduced

TABLE II
CIRCUIT PARAMETERS OF NONRECIPROCAL BPFS (REFER TO FIG. 1)

| **Case 1**: 50-to-50 Ω | **Case 2**: 20-to-50 Ω | **Case 3:** 25+j10-to-50 Ω | **Case 4:** 25+j10-to-55+j10 Ω |
|---|---|---|---|
| $R_S$ = 50 Ω, $R_L$ = 50 Ω, $X_S$ = $X_L$ = 0 Ω, Δ = 5% | $R_S$ = 20 Ω, $R_L$ = 50 Ω, $X_L$ = $X_S$ = 0 Ω, Δ = 5% | $R_S$ = 25 Ω, $X_S$ = 10 Ω, $R_L$ = 50 Ω, $X_L$ = 0 Ω, Δ = 5% | $R_S$ = 25 Ω, $X_S$ = 10 Ω, $R_L$ = 55 Ω, $X_L$ = 10 Ω, Δ = 5% |
| Resonator parameters: $Z_1$ = $Z_S$ = $Z_k$ = $Z_L$ = 70 Ω, $Z_2$ = 60 Ω, $\theta_1$ = 40°, $\theta_2$ = 25°, $\theta_0$ = 16°, $C_v$ = 6 pF, $f_{ref}$ = 1.50 GHz, $Z_{bias}$ =100 Ω, $\theta_{bias}$ = 75° | | | |
| $\theta_S$ = 39.80°, $\theta_L$ = 50°, $\theta_{k1}$ = 2.20°, $\theta_{k2}$ = 13.2° $\theta_{a1}$ = -2.23°, $\theta_{a2}$ = -12.64° | $\theta_S$ = 46.120°, $\theta_L$ = 50°, $\theta_{k1}$ = 2.23°, $\theta_{k2}$ = 13.2° $\theta_{a1}$ = -2.20°, $\theta_{a2}$ = -12.64° | $\theta_S$ = 38.08°, $\theta_L$ = 50°, $\theta_{k1}$ = 2.23°, $\theta_{k2}$ = 13.2° $\theta_{a1}$ = -2.20°, $\theta_{a2}$ = -12.64° | $\theta_S$ = 34.44°, $\theta_L$ = 35°, $\theta_{k1}$ = 2.20°, $\theta_{k2}$ = 13.24°, $\theta_{a1}$ = -2.23°, $\theta_{a2}$ = 12.35° |
| $Z_{0e1}/Z_{0o1}$ = 95.81/44.05 Ω, $Z_{0e2}/Z_{0o2}$ = 66.29/54.80 Ω | $Z_{0e1}/Z_{0o1}$ = 78.71/48.54 Ω, $Z_{0e2}/Z_{0o2}$ = 66.29/54.80 Ω | $Z_{0e1}/Z_{0o1}$ = 81.32/47.63 Ω, $Z_{0e2}/Z_{0o2}$ = 66.29/54.80 Ω | $Z_{0e1}/Z_{0o1}$ = 80.94/47.76 Ω, $Z_{0e2}/Z_{0o2}$ = 66.29/54.80 Ω |

TABLE III
PARAMETERS OF FREQUENCY TUNING STATES OF NONRECIPROCAL BPFS (REFER TO FIG. 4)

| **Case 1**: 50-to-50 Ω | | | | | **Case 2**: 20-to-50 Ω | | | **Case 3:** 25+j10-to-50 Ω | | | **Case 4:** 25+j15-to-55+j10 Ω | | |
|---|---|---|---|---|---|---|---|---|---|---|---|---|---|
| | | T1 | T2 | T3 | T1 | T2 | T3 | T1 | T2 | T3 | T1 | T2 | T3 |
| DC bias voltage and modulation parameters | $V_{dc}$ (V) | 30 | 17.5 | 8 | 30 | 17.5 | 8 | 30 | 17.5 | 8 | 30 | 17.5 | 8 |
| | $f_m$ (MHz) | 74 | 71 | 71 | 74 | 72 | 72 | 74 | 72 | 70 | 76 | 74 | 70 |
| | $V_m$ (V) | 5.50 | 4.35 | 3.55 | 5.55 | 4.40 | 3.50 | 5.60 | 4.45 | 3.25 | 5.52 | 4.40 | 3.50 |
| | $\Delta\varphi$ (Deg) | | 60 | | | 60 | | | 60 | | | 60 | |
| Results | $f_0$ (GHz) | 1.90 | 1.75 | 1.59 | 1.90 | 1.75 | 1.59 | 1.90 | 1.75 | 1.59 | 1.90 | 1.75 | 1.59 |
| | IL (dB) | 1.59 | 1.84 | 2.37 | 1.72 | 1.89 | 2.30 | 1.69 | 1.92 | 2.36 | 1.67 | 1.91 | 2.42 |
| | IX at $f_0$ (dB) | 20.54 | 20.71 | 20.31 | 20.66 | 20.36 | 20.41 | 20.10 | 20.64 | 20.45 | 20.62 | 20.44 | 20.32 |
| | $BW_{3dB\text{-}IL}$ (MHz) | 90 | 85 | 80 | 89 | 84 | 81 | 91 | 86 | 80 | 88 | 87 | 81 |
| | $BW_{20dB\text{-}IX}$ (MHz) | 48 | 45 | 45 | 48 | 46 | 44 | 48 | 44 | 43 | 48 | 46 | 44 |

IL: forward insertion loss ($|S_{21}|$), IX = reserve isolation ($|S_{12}|$), $BW_{3dB\text{-}IL}$ = forward insertion loss 3-dB bandwidth, and $BW_{20dB\text{-}IX}$ = 20-dB reverse isolation bandwidth.

from 2 to 1, and they exhibited high isolation at center frequency, although the isolation bandwidth decreased. Good compromise was reached at $f_m = 72$ MHz.

The proposed BPF exhibited strong reverse isolation when $\Delta\varphi$ was in the range of 45°–80°. When $\Delta\varphi = 80°$, high backward isolation was achieved, although out-of-band transmission zeros began to disappear and a small degradation in forward IL occured. $V_m$ also proved to be an important parameter for achieving non-reciprocity in the proposed BPF. A large $V_m$ exhibited high backward isolation, but degraded the forward IL.

As a result of these parametric studies, we conclude that the ideal modulation parameters of the proposed BPF are $f_m =$ 72 MHz (approximately equal to equiripple bandwidth of BPF), $\Delta\varphi = 60°$, and $V_m = 4.40$ V.

### F. Design Examples of Frequency Tunable Nonreciprocal BPF With Arbitrary Termination Impedances

To demonstrate the proposed arbitrary terminated frequency tunable nonreciprocal BPF, four types of nonreciprocal BPFs (50-to-50 Ω, 20-to-50 Ω, 25+$j$10-to-50 Ω, and 25+$j$10-to-55+$j$10 Ω) were designed for 0.043 dB Chebyshev response with a center frequency of 1.80 GHz and a static equiripple bandwidth of 75 MHz. Using previously described design method, the required $f_m$ was selected to be approximately 75 MHz. The progressive phase shift of the modulation signal is set as $\Delta\varphi = 60°$. The circuit parameters are provided in Table II.

Fig. 4 depicts the nonreciprocal response with center frequency tunability, which is intended to allow for the improved utilization of the limited frequency spectrum response in modern wireless communication devices. The simulated results are summarized in Table III. The center frequency of the proposed BPF is tunable by changing the dc bias voltage ($V_{\mathrm{dc}}$) and the modulation parameters ($f_m$ and $V_m$). As shown in Fig. 4, the center frequency can be tuned from 1.59 to 1.90 GHz (310 MHz) with two distinct isolation poles and two reflection zeros in all tuned states. As the results make clear, a higher $V_m$ can be used to achieve nonreciprocity at higher $f_0$.

## III. EXPERIMENTAL RESULTS

To further evaluate the proposed circuit, we prepared the experimental demonstration with four types of nonreciprocal BPFs (filter A: 50-to-50 Ω, filter B: 20-to-50 Ω, filter C: 25+$j$10 to 50 Ω, and filter D: 25+$j$10 to 55+$j$10 Ω) on a Taconic substrate with a dielectric constant of 2.2, thickness of 0.78 mm, and loss tangent of 0.0009. The corresponding BPFs were specified with a Chebyshev response with a passband ripple of 0.043 dB and a ripple bandwidth of 75 MHz at $f_0 = 1.80$ GHz. The circuit parameters of the designed BPFs are presented in Table II. The electrical lengths of the TLs are defined at $f_{\mathrm{ref}} = 1.50$ GHz. The simulation was performed using ANSYS HFSS and Keysight ADS in conjunction with a large-signal scattering analysis module. The time-varying capacitor was implemented by modulating varactor 1T362 [22].

### A. Results of Nonreciprocal BPF A: 50-to-50 Ω

Fig. 5 shows the simulation and measurement results of nonreciprocal BPF A. The measurement results (summarized in Table IV) and simulation results were consistent with each other. The center frequency of nonreciprocal BPF A can be tuned from 1.64 to 1.97 GHz (330 MHz) by varying the dc bias voltage and modulation parameter ($f_m$ and $V_m$). The measured forward IL

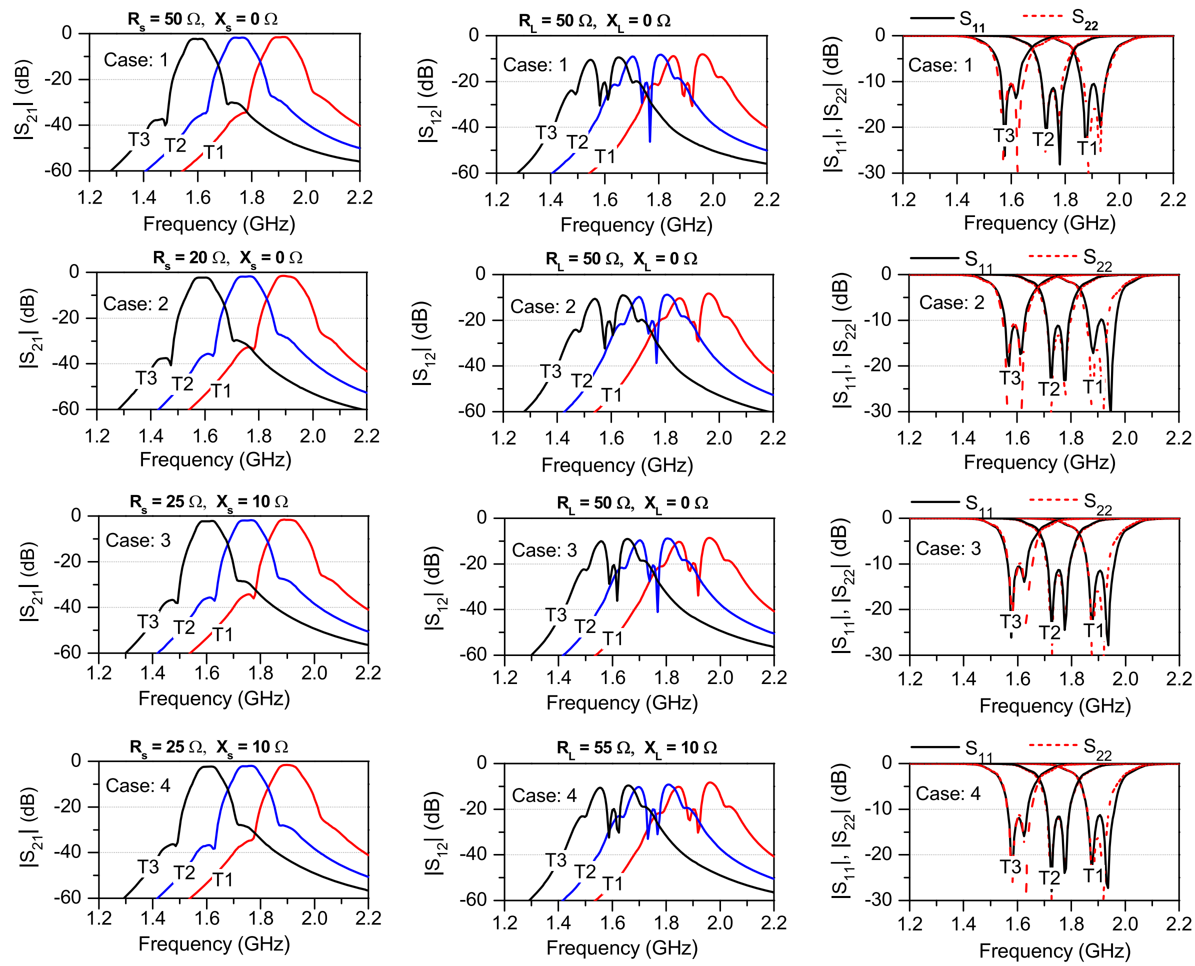


Fig. 4. Frequency responses of the proposed arbitrary terminated magnetless nonreciprocal BPFs using 1T362 varactor.

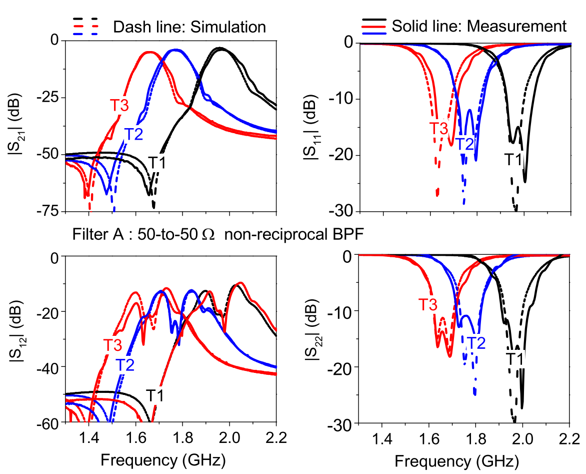


Fig. 5. Simulation and measurement results of nonreciprocal BPF A: 50-to-50 Ω (dashed line: simulation results and solid line: measurement results).

TABLE IV
MEASUREMENT RESULT OF NONRECIPROCAL BPF A

| | | T1 | T2 | T3 |
|---|---|---|---|---|
| DC bias and modulation parameters | $V_{dc}$ (V) | 35 | 15 | 8 |
| | $f_m$ (MHz) | 75 | 74 | 74 |
| | $V_m$ (V) | 2.90 | 2.4 | 2.2 |
| | $\Delta\varphi$ | 65° | 60° | 65° |
| Measured results | $f_0$ (GHz) | 1.97 | 1.77 | 1.64 |
| | IL (dB) | 3.94 | 4.40 | 4.92 |
| | IX at $f_0$ (dB) | 22.29 | 23.55 | 20.78 |
| | $BW_{3dB\text{-}IL}$ (MHz) | 87 | 90 | 97 |
| | $BW_{20dB\text{-}IX}$ (MHz) | 50 | 55 | 65 |
| | RL at $f_0$ (dB) | > 14.9 | > 12.8 | > 13.8 |
| | IIP3 (dBm) | 29.10 | 29.02 | 28.9 |

IL: forward insertion loss ($|S_{21}|$), IX = backward isolation ($|S_{12}|$).
$BW_{20dB\text{-}IX}$ = 20-dB backward isolation bandwidth.
$BW_{3dB\text{-}IL}$ = 3-dB forward insertion loss (IL) bandwidth.
RL at $f_0$: minimum input/output return loss (RL) at $f_0$.
IIP3: Third-order input intercept point.

varied from 3.94 to 4.92 dB at $f_0$. The measured forward IL increased as $f_0$ decreased due to the larger parasitic resistance of the varactor at lower $V_{dc}$.

Similarly, the backward isolation ($|S_{12}|$) is greater than 20 dB at each $f_0$ and the 20-dB isolation bandwidths are found to be greater than 50 MHz at each $f_0$. The measured input/output RLs were greater than 12.8 dB for all tuning states.

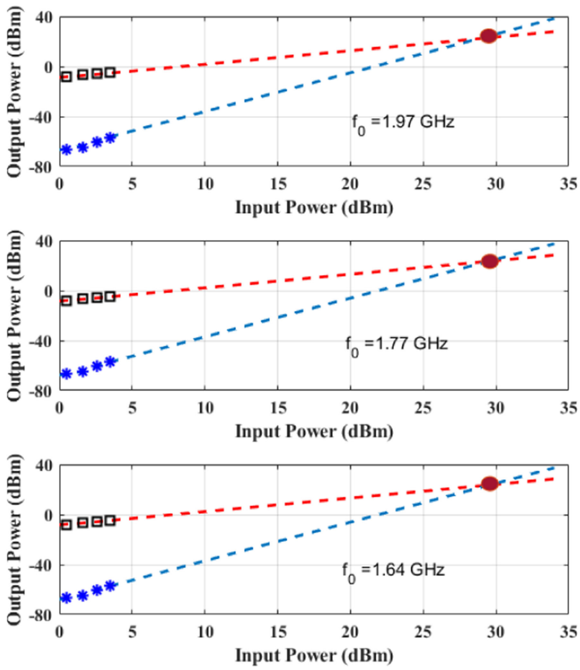


Fig. 6. Nonlinearity measurement of fabricated nonreciprocal BPF A.

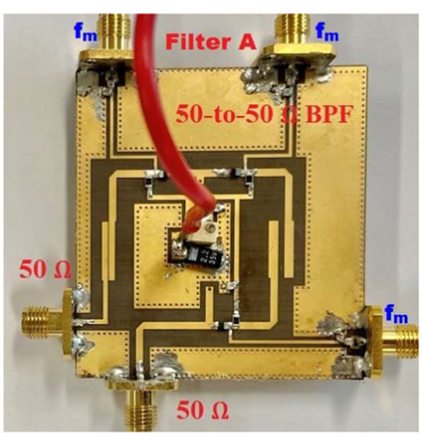


Fig. 7. Photograph of fabricated nonreciprocal BPF A: 50-to-50 Ω.

The power handling capacity and nonlinearity of the proposed nonreciprocal BPF are mainly limited by the nonlinearity of the varactors. Fig. 6 shows the measured input third-order intercept point (IIP3) of filter A. IIP3 measurement is done with two-tone input signals separated by 1 MHz. At tuning state $f_0$, the measured IIP3 is greater than 29 dBm. A photograph of the fabricated filter is provided in Fig. 7.

## B. Results of Nonreciprocal BPF B: 20-to-50 Ω

Fig. 8 shows the simulation and measurement results using nonreciprocal BPF B (20-to-50 Ω). A photograph of the fabricated filter is shown at Fig. 9. The measurements were performed as follows in case of unequal termination impedances ($Z_s$ and $Z_L \neq 50\ \Omega$) nonreciprocal BPF.

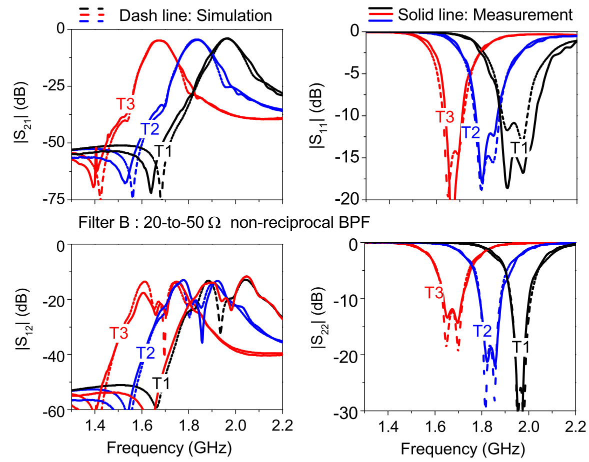


Fig. 8. Simulation and measurement results of nonreciprocal BPF B: 20-to-50 Ω (dashed line: simulation results and solid line: measurement results).

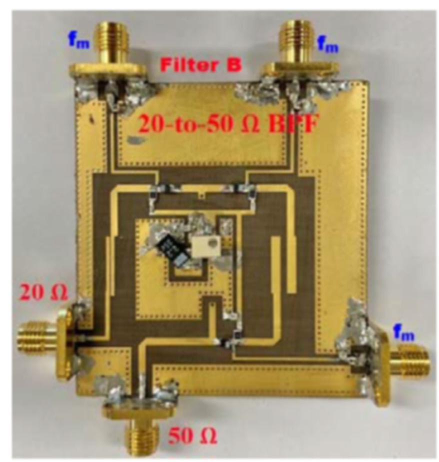


Fig. 9. Photograph of fabricated filter B: 20-to-50 Ω.

1) Calibration of network is performed for desired frequency range. After calibration, the effect of 50 Ω SMA connectors is eliminated by performing the offset of SMA connector at port 1 and port 2 of network analyzer.
2) The *S*-parameters were extracted as touchstone file using a network analyzer.
3) The touchstone file was imported into a circuit simulator, such as Keysight ADS.
4) Finally, the circuit simulator is executed by specifying the required port impedances (e.g., port $1 = 20\ \Omega$ and port $2 = 50\ \Omega$). The results are those of an arbitrary terminated nonreciprocal BPF.

The results obtained from the measurements are summarized in Table V. The measured forward IL varied from 3.98 to 4.95 dB at $f_0$. The forward 3-dB bandwidth varied from 72 to 85 MHz.

Similarly, the measured backward isolation ($|S_{12}|$) is higher than 20 dB at the tuning state frequency. The measured 20-dB isolation bandwidths are greater than 62 MHz. The input and

TABLE V
MEASUREMENT RESULT OF NONRECIPROCAL BPF B

| | | T1 | T2 | T3 |
|---|---|---|---|---|
| DC bias and modulation parameters | $V_{dc}$ (V) | 35 | 18 | 7.9 |
| | $f_m$ (MHz) | 75 | 74 | 72 |
| | $V_m$ (V) | 2.95 | 2.42 | 2.22 |
| | $\Delta\varphi$ | 65° | 65° | 60° |
| Measured results | $f_0$ (GHz) | 1.97 | 1.84 | 1.65 |
| | IL (dB) | 3.98 | 4.70 | 4.95 |
| | IX at $f_0$ (dB) | 20.1 | 23.05 | 23.03 |
| | $BW_{3dB\text{-}IL}$ (MHz) | 72 | 82 | 85 |
| | $BW_{20dB\text{-}IX}$ (MHz) | 62 | 65 | 70 |
| | RL at $f_0$ (dB) | > 16.13 | > 12.6 | > 19.52 |
| | IIP3 (dBm) | 29.06 | 28.95 | 28.82 |

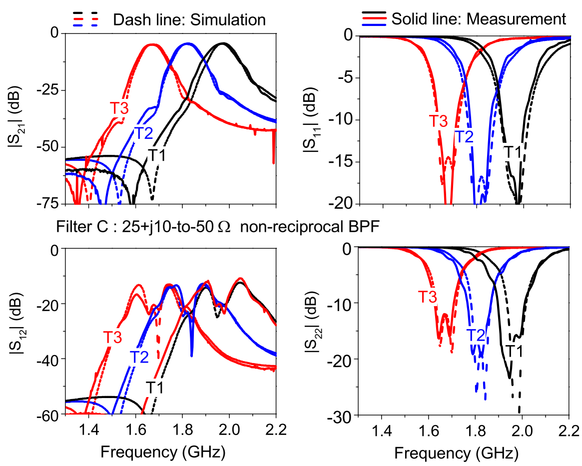


Fig. 10. Simulation and measurement results of nonreciprocal BPF C: 25+$j$10-to-50 Ω (dashed line: simulation results and solid line: measurement results).

TABLE VI
MEASUREMENT RESULTS OF NONRECIPROCAL BPF C

| | | T1 | T2 | T3 |
|---|---|---|---|---|
| DC bias and modulation parameters | $V_{dc}$ (V) | 35 | 17 | 8.1 |
| | $f_m$ (MHz) | 75 | 74 | 72 |
| | $V_m$ (V) | 2.95 | 2.42 | 2.22 |
| | $\Delta\varphi$ | 65° | 60° | 65° |
| Measured results | $f_0$ (GHz) | 1.97 | 1.80 | 1.65 |
| | IL (dB) | 3.96 | 4.61 | 4.98 |
| | IX at $f_0$ (dB) | 22.02 | 23.45 | 22.27 |
| | $BW_{3dB\text{-}IL}$ (MHz) | 85 | 90 | 88 |
| | $BW_{20dB\text{-}IX}$ (MHz) | 54 | 58 | 70 |
| | RL at $f_0$ (dB) | > 19.7 | > 19.2 | >18.8 |
| | IIP3 (dBm) | 29.02 | 28.94 | 28.91 |

output return losses are higher than 12.6 dB at the tuning state. The measured IIP3 is higher than 29 dBm.

### C. Results of Nonreciprocal BPF C: 25+j10-to-50 Ω

Fig. 10 shows the simulation and measurement results of nonreciprocal BPF C (25+$j$10-to-50 Ω). The port termination impedances were set at $R_S = 25\ \Omega$, $X_S = 10\ \Omega$, $R_L = 50\ \Omega$, and $X_L = 0\ \Omega$. The measured results are summarized in Table VI. The center frequency was tuned from 1.65 to 1.97 GHz (320 MHz).

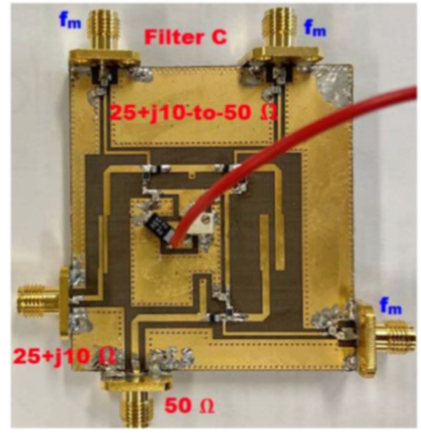


Fig. 11. Photograph of the fabricated filter C: 25+$j$10-to-50 Ω.

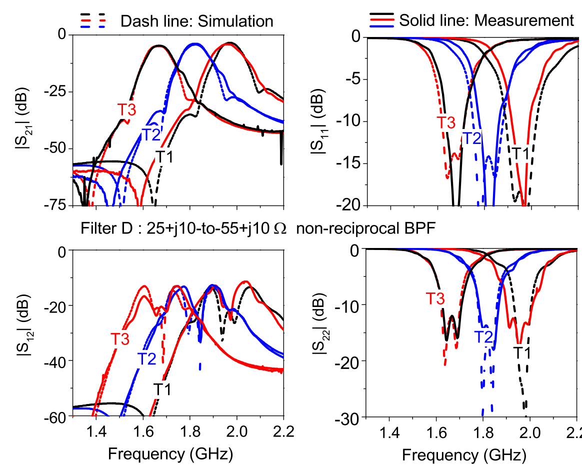


Fig. 12. Simulation and measurement results of nonreciprocal BPF D: 25+$j$10-to-55+$j$10 Ω (dashed line: simulation results and solid line: measurement results).

The measured forward IL varied from 3.96 to 4.98 dB at $f_0$. The forward 3-dB bandwidth varied from 85 to 90 MHz. Similarly, the measured backward isolation ($|S_{12}|$) was higher than 20 dB at the tuning state frequency. The measured 20-dB isolation bandwidths were found to be greater than 54 MHz. The input and output return losses were higher than 18 dB at the tuning state. The measured IIP3 was higher than 29 dBm. A photograph of fabricated filter C appears in Fig. 11.

### D. Results of Nonreciprocal BPF D: 25+j10-to-55+j10 Ω

Fig. 12 shows the simulation and measurement results of nonreciprocal BPF D (25+$j$10-to-55+$j$10 Ω). The port termination impedances were set at $R_S = 25\ \Omega$, $X_S = 10\ \Omega$, $R_L = 55\ \Omega$, and $X_L = 10\ \Omega$. The measured results are summarized in Table VII. The center frequency was tuned from 1.66 to 1.97 GHz (310 MHz). The measured forward IL varied from 3.98 to 5.01 dB at $f_0$. The forward 3-dB bandwidth varied from 85 to 92 MHz. Similarly, the measured backward isolation ($|S_{12}|$) was higher than 20 dB at the tuning state frequency. The measured 20-dB isolation bandwidths were greater than 52 MHz. The input and output

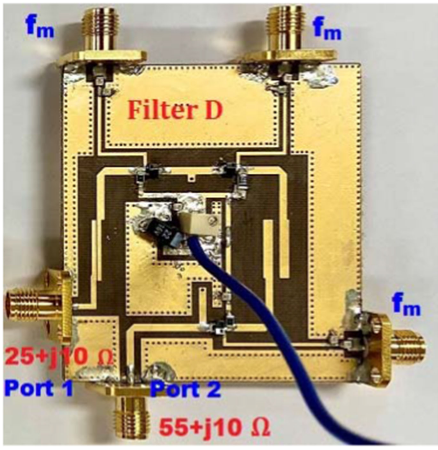


Fig. 13. Photograph of the fabricated filter D: 25+$j$10-to-55+$j$10 Ω.

TABLE VII
MEASUREMENT RESULTS OF NONRECIPROCAL BPF D

| | | T1 | T2 | T3 |
|---|---|---|---|---|
| DC bias and modulation parameters | $V_{dc}$ (V) | 35 | 21 | 8.3 |
| | $f_m$ (MHz) | 78 | 76 | 74 |
| | $V_m$ (V) | 2.96 | 2.44 | 2.21 |
| | $\Delta\varphi$ | 65° | 60° | 65° |
| Measured results | $f_0$ (GHz) | 1.97 | 1.82 | 1.66 |
| | IL (dB) | 3.98 | 4.69 | 5 |
| | IX at $f_0$ (dB) | 20.59 | 21.48 | 21.10 |
| | $BW_{3dB\text{-}IL}$ (MHz) | 92 | 89 | 85 |
| | $BW_{20dB\text{-}IX}$ (MHz) | 52 | 54 | 71 |
| | RL at $f_0$ (dB) | > 13.8 | > 15.3 | >12.3 |
| | IIP3 (dBm) | 29.10 | 28.41 | 28.6 |

TABLE VIII
PERFORMANCE COMPARISON BETWEEN THE PROPOSED BPF AND PREVIOUSLY REPORTED WORKS

| | $f_0$ (GHz) | IL (dB) | $BW_{20dB\text{-}IX}$ (MHz) | IIP3 (dBm) | CF | M |
|---|---|---|---|---|---|---|
| [10] | 1.0 | 2 | 23 | NA | No | No |
| [14] | 0.19 | 1.50 | 20 | NA | No | No |
| [15] | 0.136~0.163 | 3.7 ~ 4.1 | NA | NA | Yes | No |
| [16] | 0.27 ~ 0.31 | 1.7 ~ 4.3 | NA | NA | Yes | No |
| [17] | 0.96 | 4.50 | N/A | NA | No | No |
| [18] | 1.02 | 5.50 | NA | NA | No | No |
| [19] | 0.88~1.03 | 4.6 ~ 3.9 | 42 | 11.80 | Yes | No |
| **Filter A** | **1.64 ~ 1.97** | **3.94 ~ 4.92** | **50~65** | **29.10** | **Yes** | **Yes** |
| **Filter B** | **1.65 ~ 1.97** | **3.98 ~ 4.95** | **62~72** | **29.06** | **Yes** | **Yes** |
| **Filter C** | **1.65 ~ 1.97** | **3.96 ~ 4.98** | **54~70** | **29.02** | **Yes** | **Yes** |
| **Filter D** | **1.66 ~ 1.97** | **3.98 ~ 5.01** | **52~71** | **28.60** | **Yes** | **Yes** |

CF: Center frequency tunability and $RL_{min}$: Minimum input/output return losses.
M: Arbitrary termination impedances ($Z_S \neq Z_L$).
$BW_{20dB\text{-}IX}$: 20-dB backward isolation ($|S_{12}|$) bandwidth.
IIP3: Input third-order intercept point.

return losses were higher than 12.3 dB at the tuning state. A photograph of fabricated filter D is shown in Fig. 13.

The proposed arbitrary terminated nonreciprocal BPF is compared against those previously reported works in Table VIII. Wu *et al*. [14] demonstrated a lumped-element nonreciprocal BPF in the VHF band, which has relatively low IL due to the higher quality factor of the varactor. In addition, filter design method of Wu *et al*. [14] is only applicable for equal source and load impedance terminations ($Z_s = Z_L = 50\ \Omega$). Also, the frequency tunability of nonreciprocal response is not demonstrated. Lumped-element nonreciprocal BPFs with frequency tunability and a higher IL than currently proposed BPF were demonstrated in [15] and [16]. A microstrip line nonreciprocal BPF based on a complicated modulation circuit was demonstrated in [17], again with a higher IL than the proposed nonreciprocal BPF. In [19], a microstrip line nonreciprocal BPF based on a simpler biasing strategy was demonstrated. Notably, all previously demonstrated BPFs [14]–[19] were based on equal ($Z_s = Z_L = 50\ \Omega$) port termination impedances and none implemented a multifunctional (e.g., performing simultaneous impedance matching and frequency tunability) nonreciprocal BPF in a single device. This work, in contrast, proposed an impedance matching nonreciprocal BPF with center frequency tunability based on a simpler and more efficient modulation circuit. The proposed BPF provides not only a nonreciprocal response but also achieves impedance matching between real-to-real, real-to-complex, and complex-to-complex termination impedances. The modulation signal circuit is simple and achieves excellent nonreciprocal response in the proposed nonreciprocal BPF.

## IV. CONCLUSION

In this article, we designed and tested a frequency tunable nonreciprocal BPF. The proposed BPF design method was applicable for equal ($Z_s = Z_L = 50\ \Omega$) as well as unequal ($Z_s \neq Z_L$) termination impedances such that an impedance matching circuit and a nonreciprocal BPF can be integrated into a single circuit. This proposed modulation scheme simplified the design of nonreciprocal BPF and achieved an excellent nonreciprocal response with frequency tunability. As a proof of concept, four prototypes of microstrip line nonreciprocal BPFs (50-to-50 Ω, 20-to-50 Ω 25+$j$10-to-50 Ω, and 25+$j$10-to-55+$j$10 Ω) were designed, fabricated, and assessed with measured results consistent with those predicted by simulation and theory.

## REFERENCES


[1] S. Hong *et al.*, “Application of self-interference cancellation in 5G and beyond,” *IEEE Commun. Mag.*, vol. 52, no. 2, pp. 114–121, Feb. 2014.
[2] N. Reiskarimian, A. Nagulu, T. Dinc, and H. Krishnaswamy, “Nonreciprocal electronic devices: A hypothesis turned into reality,” *IEEE Microw. Mag.*, vol. 20, no. 4, pp. 94–111, Apr. 2019.
[3] J. Zhou *et al.*, “Integrated full duplex radios,” *IEEE Commun. Mag.*, vol. 55, no. 4, pp. 142–151, Apr. 2017.
[4] C. E. Fay and R. L. Comstock, “Operation of the ferrite junction circulator,” *IEEE Trans. Microw. Theory Techn.*, vol. MTT-13, no. 1, pp. 15–27, Jan. 1965.
[5] C. K. Seewald and J. R. Bray, “Ferrite-filled antisymmetrically biased rectangular waveguide isolator using magnetostatic surface wave modes,” *IEEE Trans. Microw. Theory Techn.*, vol. 58, no. 6, pp. 1493–1501, Jun. 2010.
[6] S. Tanaka, N. Shimomura, and K. Ohtake, “Active circulators: The realization of circulators using transistors,” *Proc. IEEE*, vol. 53, no. 3, pp. 260–267, Mar. 1965.
[7] T. Kodera, D. L. Sounas, and C. Caloz, “Magnetless nonreciprocal metamaterial (MNM) technology: Application to microwave components,” *IEEE Trans. Microw. Theory Techn.*, vol. 61, no. 3, pp. 1030–1042, Mar. 2013.
[8] C. Caloz, A. Alù, S. Tretyakov, D. Sounas, K. Achouri, and Z.-L. Deck-Léger, “Electromagnetic nonreciprocity,” *Phys. Rev. Appl.*, vol. 10, no. 4, 2018, Art. no. 047001.

[9] N. A. Estep, D. L. Sounas, and A. Alù, "Magnetless microwave circulators based on spatiotemporally modulated rings of coupled resonators," *IEEE Trans. Microw. Theory Techn.*, vol. 64, no. 2, pp. 502–518, Feb. 2016.
[10] A. Kord, D. L. Sounas, Z. Xiao, and A. Alu, "Broadband cyclic-symmetric magnetless circulators and theoretical bounds on their bandwidth," *IEEE Trans. Microw. Theory Techn.*, vol. 66, no. 12, pp. 5472–5481, Dec. 2018.
[11] Y. Yu *et al.*, "Radio frequency magnet-free circulators based on spatiotemporal modulation of surface acoustic wave filters," *IEEE Trans. Microw. Theory Techn.*, vol. 67, no. 12, pp. 4773–4782, Dec. 2019.
[12] A. Kord, D. L. Sounas, and A. Alu, "Pseudo-linear time-invariant magnetless circulators based on differential spatiotemporal modulation of resonant junctions," *IEEE Trans. Microw. Theory Techn.*, vol. 66, no. 6, pp. 2731–2745, Jun. 2018.
[13] N. Reiskarimian and H. Krishnaswamy, "Magnetic-free non-reciprocity based on staggered commutation," *Nat. Commun.*, vol. 7, Apr. 2016, Art. no. 11217.
[14] X. Wu, X. Liu, M. D. Hickle, D. Peroulis, J. S. Gomez-Dıaz, and A. Alvarez Melcon, "Isolating bandpass filters using time-modulated resonators," *IEEE Trans. Microw. Theory Techn.*, vol. 67, no. 6, pp. 2331–2345, Jun. 2019.
[15] D. Simpson and D. Psychogiou, "Magnet-less non-reciprocal bandpass filters with tunable center frequency," in *Proc. 49th Eur. Microw. Conf.*, 2019, pp. 460–463.
[16] D. Simpson and D. Psychogiou, "Fully-reconfigurable non-reciprocal bandpass filters," in *Proc. IEEE/MTT-S Int. Microw. Symp.*, 2020, pp. 807–810.
[17] A. Alvarez Melcon, X. Wu, J. Zang, X. Liu, and J. S. Gomez-Diaz, "Coupling matrix representation of nonreciprocal filters based on time-modulated resonators," *IEEE Trans. Microw. Theory Techn.*, vol. 67, no. 12, pp. 4751–4763, Dec. 2019.
[18] X. Wu, M. Nafe, A. Alvarez Melcon, J. S. Gomez-Diaz, and X. Liu, "A non-reciprocal microstrip bandpass filter based on spatio-temporal modulation," in *Proc. IEEE MTT-S Int. Microw. Symp.*, Jun. 2019, pp. 9–12, doi: 10.1109/MWSYM.2019.8700732.
[19] X. Wu, M. Nafe, A. Alvarez Melcon, J. S. Gomez-Diaz, and X. Liu, "Frequency tunable non-reciprocal bandpass filter using time-modulated microstrip $\lambda_g/2$ resonators," *IEEE Trans. Circuits Syst. II, Exp. Briefs,* vol. 68, no. 2, pp. 667–671, Feb. 2021.
[20] P. Kim and Y. Jeong, "A new synthesis and design approach of a complex termination impedance bandpass filter," *IEEE Trans. Microw. Theory Techn.*, vol. 67, no. 6, pp. 2346–2354, Jun. 2019.
[21] P. Kim, G. Chaudhary, and Y. Jeong, "Wide-stopband and high selectivity step impedance resonator bandpass filter using T-network and antiparallel coupled lines," *IET Microw., Antennas Propag.*, vol. 13, no. 11, pp. 1916–1920, 2019.
[22] 1T362: Silicon variable capacitance diode, Sony Corp., Tokyo, Japan.

**Girdhari Chaudhary** (Member, IEEE) received the B.E. and M.Tech. degrees in electronics and communication engineering from Nepal Engineering College, Kathmandu, Nepal, and the Malaviya National Institute of Technology, Jaipur, India, in 2004 and 2007, respectively, and the Ph.D. degree in electronics engineering from Jeonbuk National University, Jeonju-si, South Korea, in 2013.

He is currently an Assistant Research Professor with the Division of Electronics Engineering, Jeonbuk National University, South Korea. He was a Principal Investigator on an independent project through the Basic Science Research Program administrated by the National Research Foundation (NRF) and funded by the Ministry of Education. His research interests include multiband tunable passive circuits, in-band full duplex systems, and high-efficiency power amplifiers and applications of negative group delay circuits.

Dr. Chaudhary was a recipient of the BK21 PLUS Research Excellence Award 2015 by the Korean Ministry of Education, a Korean Research Fellowship (KRF) through the NRF funded by the Ministry of Science and ICT.

**Yongchae Jeong** (Senior Member, IEEE) received the B.S.E.E., M.S.E.E., and Ph.D. degrees in electronics engineering from Sogang University, Seoul, South Korea, in 1989, 1991, and 1996, respectively.

Between 1991 and 1998, he was a Senior Engineer with Samsung Electronics, Seoul. In 1998, he joined the Division of Electronics Engineering, Jeonbuk National University, Jeonju-si, South Korea. During July 2006 and December 2007, he was a Visiting Professor with the Georgia Institute of Technology. He is a Professor as well as a member of IT Convergence Research Center. With Jeonbuk National University, he was a Director of HOPE-IT Human Resource Development Center of BK21 PLUS. He is Jeonbuk National University's Vice-President of Planning and continues to teach and research passive and active microwave circuits, mobile and satellite base-station RF system, periodic defected transmission lines, negative group delay circuits and their applications, in-band full duplex radio, and RFIC design. He has authored and coauthored more than 260 papers in international journals and conference proceedings.

Dr. Jeong is a member of Korea Institute of Electromagnetic Engineering and Science.